Inorg. Chem. **2002**, *41*, 3570–3577

Spin Dimer Analysis of the Spin Exchange Interactions in Paramelaconite Cu_4O_3 and Its Analogue $Ag_2Cu_2O_3$ and the Spin Ordering of the Cu_2O_3 Spin Lattice Leading to Their Magnetic Phase Transitions

M.-H. Whangbo* and H.-J. Koo

Department of Chemistry, North Carolina State University, Raleigh, North Carolina 27695-8204

Received February 19, 2002

The magnetic structures of the Cu_2O_3 spin lattices present in Cu_4O_3 and $Ag_2Cu_2O_3$ were analyzed by studying their spin exchange interactions on the basis of spin dimer analysis. Calculations of spin exchange parameters were calibrated by studying $LiCuVO_4$ whose intrachain and interchain antiferromagnetic spin exchange parameters are known experimentally. The magnetic phase transition of Cu_4O_3 at 42.3 K doubles the unit cell along each crystallographic direction. The spin arrangements of the Cu_2O_3 lattice consistent with this experimental observation are different from conventional antiferromagnetic ordering. Our analysis indicates that spin fluctuation should occur in Cu_4O_3, low-dimensional magnetism should be more important than magnetic frustration in Cu_4O_3, and $Ag_2Cu_2O_3$ and Cu_4O_3 should have similar structural and magnetic properties.

1. Introduction

Paramelaconite Cu_4O_3[1] is a mineral that shows puzzling magnetic properties.[2] The Cu_2O_3 lattice of spin-$^1/_2$ Cu^{2+} ions results from Cu_4O_3 when the diamagnetic Cu^+ ions are removed (Figure 1). A neutron diffraction study[2] reveals that Cu_4O_3 undergoes a magnetic phase transition below 42.3 K leading to a supercell (2*a*, 2*b*, 2*c*); namely, the phase transition doubles the unit cell along each crystallographic direction.[2] The intensity of a magnetic reflection was reported to show a temperature dependence that can be interpreted in terms of either low-dimensional magnetism or magnetic frustration.[2] The crystal structure[1] and the magnetic properties[2] of Cu_4O_3 have been studied using single-crystal mineral samples.[3] So far, it is unknown how to synthesize homogeneous samples of Cu_4O_3, although extraction of copper or its oxides with concentrated aqueous ammonia was found to produce a mixture of Cu_4O_3, Cu_2O, and CuO.[4] Mineral samples of Cu_4O_3 contain CuO and other unknown magnetic impurities,[2] so a quantitative analysis of the magnetic susceptibility of Cu_4O_3 is complicated. Nevertheless, the magnetic susceptibility shows a maximum around 75 K and a sharp decrease below 42.3 K,[2] which suggest an antiferromagnetic phase transition. $Ag_2Cu_2O_3$ is isostructural and isoelectronic with Cu_4O_3.[5−7] The structure of $Ag_2Cu_2O_3$ results when the Cu^+ ions of Cu_4O_3 are replaced with Ag^+ ions; that is, $Ag_2Cu_2O_3$ has the same Cu_2O_3 spin lattice as found for Cu_4O_3. The magnetic susceptibility of $Ag_2Cu_2O_3$ shows a broad maximum at ∼80 K[6,7] and a sharp decrease below 60 K,[6] which again suggest an antiferromagnetic phase transition. So far, no study has been reported concerning the magnetic structure of $Ag_2Cu_2O_3$ below 60 K.

There are several important questions concerning the magnetic structures of Cu_4O_3 and $Ag_2Cu_2O_3$. It should be noted that each CuO_2 ribbon chain has two spin-$^1/_2$ Cu^{2+} ions per unit cell (Figure 1b) so that an antiferromagnetic

* To whom correspondence should be addressed. E-mail: mike_whangbo@ncsu.edu.

(1) O'Keeffe, M.; Bovin, J.-O. *Am. Mineral.* **1978**, *63*, 180.
(2) Pinsard-Gaudart, J.; Rodriguez-Carvajal, J.; Gukasov, A.; Monod, P.; Dechamps, M.; Jegoudez, J. Propriétés magnétiques de Cu_4O_3-Un reseau pyrochlore à spin 1/2. Presented at Colloque Oxydes à Propriétés Remarquables: Ordre de spins, ordre de charges et phénomènes coopératifs; Berthier, C., Collin, G., Doumerc, J.-P., organizers; Bombannes, June 6−8, 2001. The abstracts of the meeting are collected in the report GDR 2069.
(3) Smithsonian 112878; Smithsonian Institution: Washington, DC.
(4) Morgan, P. E. D.; Partin, D. E.; Chamberland, B. L.; O'Keeffe, M. *J. Solid State Chem.* **1996**, *121*, 33.
(5) Gómez-Romero, P.; Tejada-Rosales, E. M.; Palacín, M. R. *Angew. Chem., Int. Ed.* **1999**, *38*, 524.
(6) Adelsberger, K.; Curda, J.; Vensky, S.; Jansen, M. *J. Solid State Chem.* **2001**, *158*, 82.
(7) Tejada-Rosales, E. M.; Rodriguez-Carvajal, J.; Palacin, M. R.; Gómez-Romero, P. *Mater. Sci. Forum* **2001**, *378*−*381*, 606.

10.1021/ic020141x CCC: $22.00
Published on Web 06/01/2002

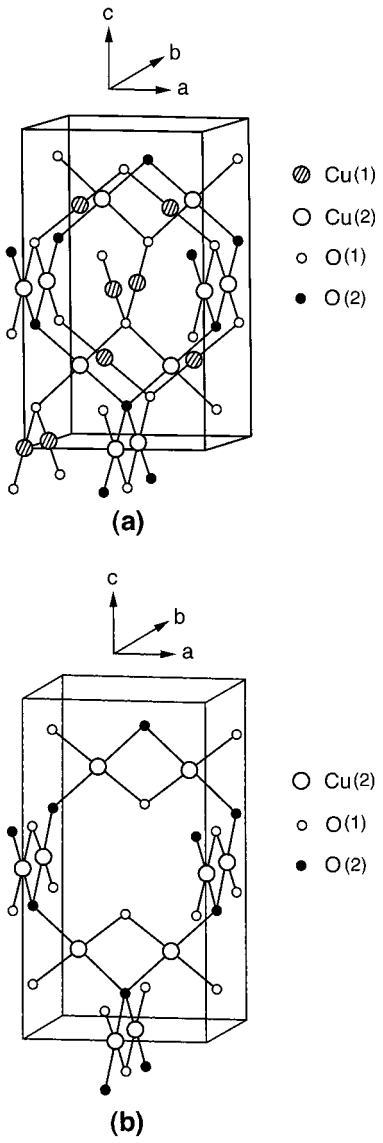

Figure 1. (a) Perspective view of the crystal structure of Cu_4O_3. (b) Perspective view of the Cu_2O_3 spin lattice of Cu_4O_3.

ordering such as $(\uparrow\downarrow)_\infty$ along each chain does not double the unit cell along the *a*- and *b*-direction. There are four layers of CuO_2 ribbon chains in a unit cell of the Cu_2O_3 lattice (Figure 1b). Thus, an antiferromagnetic ordering such as $(\uparrow\downarrow\uparrow\downarrow)_\infty$ in the successive layers of CuO_2 ribbon chains does not double the unit cell along the *c*-direction. It is quite challenging to find what kind of spin ordering takes place in the Cu_2O_3 lattice of Cu_4O_3 below 42.3 K to double the unit cell along each crystallographic direction and see if the magnetic phase transition associated with such a spin ordering can be considered as an antiferromagnetic phase transition. So far, it has not been studied whether the spin exchange interactions of the Cu_2O_3 lattice support the suggestion[2] that low-dimensional magnetism or magnetic frustration is responsible for the observed temperature dependence of a magnetic reflection intensity in Cu_4O_3, and whether there exists an alternative explanation for this experimental observation. It is important to investigate if the answers to these questions are equally applicable to $Ag_2Cu_2O_3$. In the present work, we probe these questions by analyzing the spin exchange interactions of the Cu_2O_3 lattices in $Ag_2Cu_2O_3$ and Cu_4O_3 on the basis of spin dimer analysis.

Our work is organized as follows: The essence of spin dimer analysis is briefly described in Section 2. The Cu_2O_3 lattices of Cu_4O_3 and $Ag_2Cu_2O_3$ are examined in Section 3 to identify their spin dimers (i.e., structural units containing two adjacent spin sites). In Section 4, we discuss how to calibrate our calculations of spin exchange parameters. In Section 5, we probe the spin ordering of Cu_4O_3 leading to its magnetic phase transition and its implications concerning low-dimensional magnetism and magnetic frustration. We then compare the spin exchange interactions of Cu_4O_3 and $Ag_2Cu_2O_3$. Important results of our work are summarized in Section 6.

2. Spin Dimer Analysis

Theoretically, physical properties of a magnetic solid are described in terms of a spin-Hamiltonian. This phenomenological Hamiltonian is expressed as a sum of pairwise spin exchange interactions. In terms of first-principles electronic structure calculations, the strengths of spin exchange interactions (i.e., spin exchange parameters *J*) can be calculated in two ways: (a) electronic structure calculations for the high- and low-spin states of spin dimers (i.e., structural units consisting of two spin sites)[8−10] and (b) electronic band structure calculations for various ordered spin arrangements of a magnetic solid.[11] For magnetic solids with large and complex unit cell structures, these quantitative methods become difficult to apply. In understanding physical properties of magnetic solids, however, it is often sufficient to estimate the relative magnitudes of their *J* values.[12−18] In general, a spin exchange parameter *J* can be written as $J = J_F + J_{AF}$, where the ferromagnetic term J_F (>0) is small so that the spin exchange becomes ferromagnetic (i.e., $J > 0$) when the antiferromagnetic term J_{AF} (<0) is negligibly small in magnitude. Spin exchange interactions of magnetic solids are mostly antiferromagnetic (i.e., $J < 0$) and can be discussed by focusing on the antiferromagnetic terms J_{AF}.[13−18]

Suppose that each spin site of a magnetic solid contains one unpaired electron, the two spin sites of a spin dimer are equivalent, and the two spin sites of a spin dimer are represented by nonorthogonal magnetic orbitals (i.e., singly

(8) Illas, F.; Moreira, I. de P. R.; de Graaf, C.; Barone, V. *Theor. Chem. Acc.* **2000**, *104*, 265 and the references therein.
(9) Noodleman, L. *J. Chem. Phys.* **1981**, *74*, 5737.
(10) Dai, D.; Whangbo, M.-H. *J. Chem. Phys.* **2001**, *114*, 2887.
(11) Derenzo, S. E.; Klitenberg, M. K.; Weber, M. J. *J. Chem. Phys.* **2000**, *112*, 2074 and the references therein.
(12) Kahn, O. *Molecular Magnetism*; VCH Publishers: Weinheim, 1993.
(13) Hay, P. J.; Thibeault, J. C.; Hoffmann, R. *J. Am. Chem. Soc.* **1975**, *97*, 4884.
(14) Koo, H.-J.; Whangbo, M.-H. *J. Solid State Chem.* **2000**, *151*, 96.
(15) Koo, H.-J.; Whangbo, M.-H. *J. Solid State Chem.* **2000**, *153*, 263.
(16) Koo, H.-J.; Whangbo, M.-H. *Inorg. Chem.* **2000**, *39*, 3599.
(17) Koo, H.-J.; Whangbo, M.-H. *Inorg. Chem.* **2001**, *40*, 2169 and the references therein.
(18) Dai, D.; Koo, H.-J.; Whangbo, M.-H. In *Solid State Chemistry of Inorganic Materials III*; Geselbracht, M. J., Greedan, J. E., Johnson, D. C., Subramanian, M. A., Eds.; Materials Research Society: Warrendale, PA, 2001; MRS Symposium Proceedings, Vol. 658, GG5.3.1−5.3.11 and the references therein.

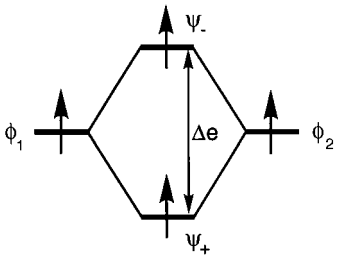

Figure 2. Orbital interaction diagram between two magnetic sites in a spin dimer, where the spin−orbital interaction energy Δe is defined as the energy difference of the two singly filled orbitals of the spin dimer.

occupied molecular orbitals of the spin monomers) ϕ_1 and ϕ_2. Provided that S_{12} and Δe are, respectively, the overlap integral and the spin−orbital interaction energy (Figure 2) between ϕ_1 and ϕ_2, then the antiferromagnetic term J_{AF} is related to S_{12} and Δe as $J_{AF} \propto -S_{12}\Delta e \propto -(\Delta e)^2$.[12,13] In recent years, spin exchange interactions of various magnetic solids[14−18] have been examined in terms of the Δe values calculated for their spin dimers using the extended Hückel method.[19,20]

Because J_{AF} is proportional to $-(\Delta e)^2$, it can be written as $J_{AF} = -\gamma(\Delta e)^2$. For antiferromagnetic spin exchange interactions, the proportionality constant γ can be estimated by comparing the calculated $(\Delta e)^2$ values with the corresponding J values determined experimentally. The energy Δe is equivalent to $2t$, where t is the hopping integral between spin sites (i.e., the resonance integral between ϕ_1 and ϕ_2). From the relationship[12,13,21]

$$J_{AF} = -4t^2/U_{eff} = -(\Delta e)^2/U_{eff}$$

we obtain $\gamma = 1/U_{eff}$, where U_{eff} is the effective on-site repulsion. For a set of closely related magnetic solids, the U_{eff} value would be nearly constant and hence could be used to approximate antiferromagnetic J by $-(\Delta e)^2/U_{eff}$.

3. Spin Dimers of the Cu_2O_3 Lattice

The Cu_2O_3 lattice can be regarded as constructed from CuO_2 ribbon chains, which are made up of edge-sharing CuO_4 square planes (Figure 1b). Each CuO_4 square plane (Figure 3a) is a spin monomer (i.e., a structural unit containing a spin site) of the Cu_2O_3 lattice. In the Cu_2O_3 lattice, layers of CuO_2 ribbon chains parallel to the a-direction alternate with layers of CuO_2 ribbon chains parallel to the b-direction. In each layer of CuO_2 ribbon chains, the plane of each ribbon chain is perpendicular to the layer. The ribbon chains between adjacent layers are condensed by sharing their O(2) atoms such that each O(2) atom is located at the center of the Cu_4 tetrahedron made up of the four surrounding Cu(2) atoms. (In passing, we note that copper oxide CuO is also made up of corner-sharing CuO_2 ribbon chains[22] and that CuO exhibits complex spin dynamics[23] and charge−spin−orbital correlation.[24])

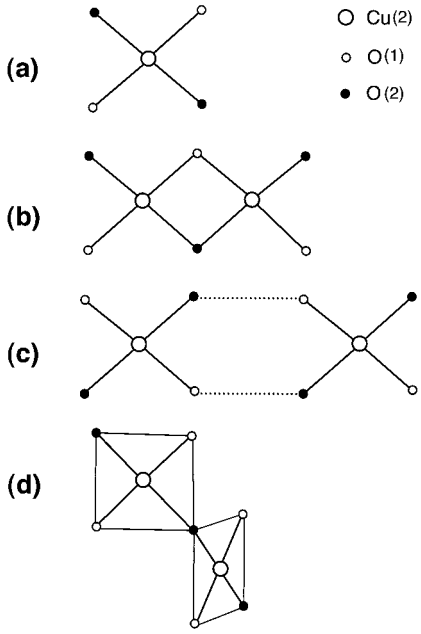

Figure 3. Spin carrying units of the Cu_2O_3 lattices in Cu_4O_3 and $Ag_2Cu_2O_3$. (a) Spin monomer CuO_4. (b) Spin dimer Cu_2O_6 for the intrachain NN interaction. (c) Spin dimer Cu_2O_8 for the intrachain NNN interaction. (d) Spin dimer Cu_2O_7 for the interchain NN interaction.

Table 1. Geometrical Parameters Associated with the Spin Dimers of the Cu_2O_3 Lattices Present in Cu_4O_3 and $Ag_2Cu_2O_3$[a]

geometrical parameter	Cu_4O_3[b]	$Ag_2Cu_2O_3$[c]
Cu(2)−O(1)	1.966	1.857
Cu(2)−O(2)	1.916	1.987
O(1)···O(2) (intrachain)	2.920	2.946
∠Cu(2)−O(1)−Cu(2) (intrachain)	95.8	104.8
∠Cu(2)−O(2)−Cu(2) (intrachain)	99.2	95.5
∠Cu(2)−O(1)···O(2) (intrachain)	136.4	142.9
∠Cu(2)−O(2)···O(1) (intrachain)	141.1	135.3
∠Cu(2)−O(2)−Cu(2) (interchain)	114.8	116.9

[a] The distances in angstrom units and the angles in degrees. [b] Taken from the crystal structure of ref 1. [c] Taken from the crystal structure of ref 6.

There are two kinds of Cu−O−Cu superexchange paths to consider in the Cu_2O_3 lattice, that is, the intrachain and interchain Cu−O−Cu paths. As summarized in Table 1, the interchain Cu−O−Cu paths have a significantly larger ∠Cu−O−Cu angle than do the intrachain Cu−O−Cu paths. This difference has a profound effect on the relative strengths of the interchain and intrachain superexchange interactions (see later). In each CuO_4 square plane, two O(1) atoms are located at diagonally opposite corners, and two O(2) atoms occupy the remaining corners. Thus, the O(1) and O(2) atoms alternate on one edge of each CuO_2 ribbon chain, but the O(2) and O(1) atoms do on the opposite edge. This structural feature of opposite senses of O(1) and O(2) alternation plays a vital role in the spin ordering along the c-direction (see later).

(19) Hoffmann, R., *J. Chem. Phys*. **1963**, *39*, 1397.
(20) Our calculations were carried out by employing the *CAESAR* program package (Ren, J.; Liang, W.; Whangbo, M.-H. *Crystal and Electronic Structure Analysis Using CAESAR*; 1998; http://www.PrimeC.com/.).
(21) This expression is valid when spin exchange parameters of a spin Hamiltonian are written as J instead of $2J$.
(22) Åsbrink, S.; Norrby, L.-J. *Acta Crystallogr., Sect. B* **1970**, *26*, 8.
(23) Eroles, J. *Phys. Rev. B* **2002**, *65*, 92404 and the references therein.
(24) Zheng, X.-G.; Xu, C.-N.; Tanaka, E.; Tomokio, Y.; Yamada, H.; Soejima, Y.; Yamamura, Y.; Tsuji, T. *J. Phys. Soc. Jpn*. **2001**, *70*, 1054 and the references therein.

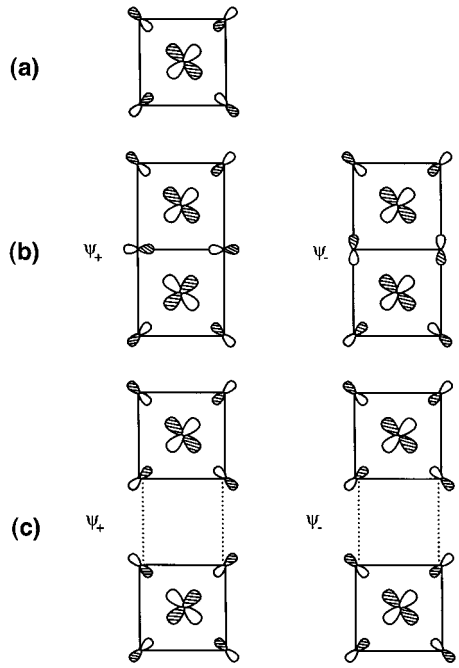

Figure 4. Magnetic orbitals of (a) the spin monomer CuO_4, (b) the spin dimer Cu_2O_6 for the intrachain NN interaction, and (c) the spin dimer Cu_2O_8 for the intrachain NNN interaction.

In calculating the Δe values for various spin exchange paths of the Cu_2O_3 lattice, it is necessary to specify the corresponding spin dimers. Within each CuO_2 ribbon chain, the spin dimer for the nearest-neighbor (NN) interaction is the edge-sharing dimer Cu_2O_6 (Figure 3b), and that for the next-nearest-neighbor (NNN) interaction is the dimer Cu_2O_8 made up of two isolated monomers (Figure 3c). Between adjacent corner-sharing CuO_2 ribbon chains, the spin dimer for the NN interaction is the corner-sharing dimer Cu_2O_7, in which the planes of the two CuO_4 units are perpendicular to each other (Figure 3d). The intrachain NN spin exchange has two Cu−O−Cu superexchange paths, but the interchain NN spin exchange has one. The intrachain NNN spin exchange has two Cu−O···O−Cu super-superexchange paths. Table 1 summarizes some geometrical parameters associated with the spin dimers of the Cu_2O_3 lattices in Cu_4O_3 and $Ag_2Cu_2O_3$. Note that the two Cu−O−Cu intrachain superexchange paths are considerably more asymmetric in $Ag_2Cu_2O_3$ than in Cu_4O_3 and that the interchain Cu−O−Cu superexchange path has a slightly larger ∠Cu−O−Cu angle in $Ag_2Cu_2O_3$ than in Cu_4O_3.

4. Magnetic Orbital Tails and Calibration of Spin Exchange Parameter Calculations

In the magnetic orbital of a spin monomer CuO_4 unit (i.e., the molecular orbital containing an unpaired spin) (Figure 4a), the Cu x^2-y^2 orbital is combined out-of-phase with the O 2p orbitals. In general, such O 2p orbital contributions to magnetic orbitals are small, but they are important in determining the magnitude of spin−orbital interaction energies Δe.[14−18] For example, the Δe of the intrachain NN spin exchange is equal to the energy difference between the two magnetic orbitals shown in Figure 4b and depends critically upon the overlap of the Cu x^2-y^2 orbital with the O 2p orbitals of the Cu−O−Cu superexchange paths. Likewise, the Δe of the intrachain NNN spin exchange is given by the energy difference between the two magnetic orbitals shown in Figure 4c and depends sensitively on the overlap between the O 2p orbitals of the O···O contacts in the Cu−O···O−Cu super-superexchange paths. To reproduce the trends in spin exchange interactions of magnetic solids using Δe values obtained from extended Hückel calculations, it is found[14−18] necessary to employ double-ζ Slater type orbitals (DZ STOs)[25] for both the 3d orbitals of the transition metal and the s/p orbitals of the surrounding ligand atoms.

Table 2. Exponents ζ_i and Valence Shell Ionization Potentials H_ii of Slater-type Orbitals χ_i Used for Extended Hückel Tight-binding Calculation[a]

atom	χ_i	H_{ii} (eV)	ζ_i	C_i[b]	ζ_i'	C_i'[b]
Cu	4s	−11.4	2.151	1.0		
Cu	4p	−6.06	1.370	1.0		
Cu	3d	−14.0	7.025	0.4473	3.004	0.6978
O	2s	−32.3	2.688	0.7076	1.675	0.3745
O	2p	−14.8	3.694	0.3322	1.659[c]	0.7448

[a] H_{ii}'s are the diagonal matrix elements $\langle\chi_i|H^{\text{eff}}|\chi_i\rangle$, where H^{eff} is the effective Hamiltonian. In our calculations of the off-diagonal matrix elements $H_{ij} = \langle\chi_i|H^{\text{eff}}|\chi_j\rangle$, the weighted formula was used. See: Ammeter, J.; Bürgi, H.-B.; Thibeault, J.; Hoffmann, R. *J. Am. Chem. Soc.* **1978**, *100*, 3686. [b] Coefficients used in the double-ζ Slater-type orbital expansion. [c] The calibration of our calculations was carried out using $\zeta'(x) = 1.659(1 + x)$ as a function of $x \geq 0$. The optimum ζ' value is found for $x = 0.125$ (see the text).

The atomic orbital parameters of Cu and O employed for our extended Hückel tight-binding calculations are listed in Table 2. For magnetic solids consisting of CuO_2 ribbon chains, our calculations using these parameters, which are determined from atomic orbital calculations,[25] lead to an unreasonable result that the intrachain NN interaction is weaker than the intrachain NNN interaction. This result originates essentially from the fact that the O 2p orbital tail is too diffuse. The radial part of the O 2p orbital, $\chi_{2p}(r)$, is written as

$$\chi_{2p}(r) = r[C \exp(-\zeta r) + C' \exp(-\zeta' r)]$$

where the exponents ζ and ζ' describe contracted and diffuse STOs, respectively (i.e., $\zeta > \zeta'$). The diffuse STO provides an orbital tail that enhances overlap between O atoms in the short O···O contacts of the Cu−O···O−Cu super-super-exchange paths as well as that between the Cu 3d and O 2p orbitals of the Cu−O−Cu superexchange paths. The Δe values are affected most sensitively by the exponent ζ' of the diffuse STO of the O 2p orbital. To determine the appropriate ζ' value, it is necessary to carry out spin dimer analysis for a magnetic solid that has spin dimers similar to those found in Cu_4O_3 and whose antiferromagnetic spin exchange parameters are known experimentally.

The magnetic solid $LiCuVO_4$[26−29] has spin-$^1/_2$ Cu^{2+} ions as the only magnetic ions and consists of isolated CuO_4

(25) Clementi, E.; Roetti, C. *At. Data Nucl. Data Tables* **1974**, *14*, 177.
(26) Lafontaine, M. A.; Leblanc, M.; Frey, G. *Acta Crystallogr., Sect. C* **1989**, *45*, 1205.
(27) Kanno, R.; Kawamoto, Y.; Takeda, Y.; Hasegawa, M.; Yamamoto, O.; Kinimura, N. *J. Solid State Chem.* **1992**, *96*, 397.
(28) Vasil'ev, A. N. *JETP Lett.* **1999**, *69*, 876.

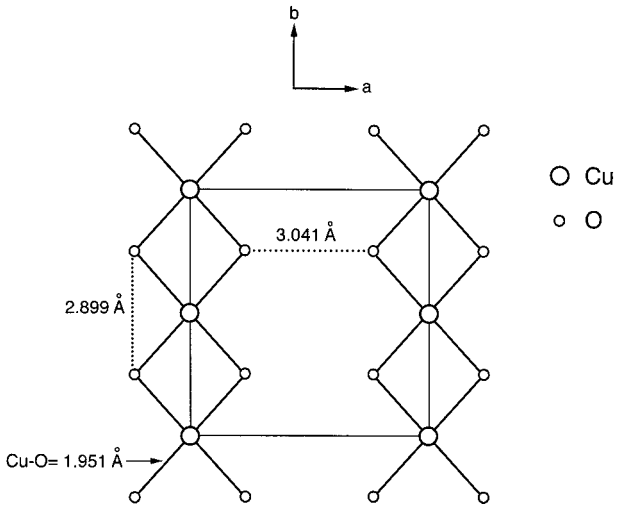

Figure 5. Arrangement of two adjacent CuO_2 ribbon chains present in every layer of CuO_2 ribbon chains in the magnetic solid $LiCuVO_4$.

octahedral chains aligned along the crystallographic *b*-direction.[26,27] Each CuO_4 octahedral chain is made up of edge-sharing CuO_6 octahedra, and every CuO_6 octahedron is axially elongated with the axial Cu−O bonds perpendicular to the chain direction. Thus, the magnetic orbital of each CuO_6 octahedron is contained in the equatorial CuO_4 square plane, and such CuO_4 square planes form a CuO_2 ribbon chain. Thus, the spin lattice (i.e., the lattice containing magnetic orbitals) of $LiCuVO_4$ consists of layers of CuO_2 ribbon chains[26,27] as depicted in Figure 5, where the CuO_2 ribbons are contained in the plane of the layer. Consequently, there occur three spin exchange interactions of interest, that is, the intrachain NN interaction (J_1), the intrachain NNN interaction (J_2), and the interchain NN interaction (J_3). As far as their spin dimers are concerned, the interchain NN and the intrachain NNN interactions are similar in nature because both have two Cu−O···O−Cu super-superexchange paths contained in the plane of their magnetic orbitals (e.g., Figure 3c). It is known experimentally[28,29] that J_1 and J_3 are antiferromagnetic with values $J_1/k_B = -22.5$ K and $J_3/k_B = -1.3$ K.

To determine the ζ' value of $\chi_{2p}(r)$ that reproduces the experimental J_3/J_1 ratio found for $LiCuVO_4$, we examine how the Δe values for the J_1, J_2, and J_3 interactions change when the ζ' value is gradually increased as $\zeta'(x) = 1.659(1 + x)$ (see Table 2), that is, as the diffuseness of the O 2p orbital tail is gradually decreased ($x \geq 0$). Figure 6 shows that the intrachain NN interaction increases gradually with increasing x whereas both the interchain NN and the intrachain NNN interactions exhibit the opposite trend. The calculated $(\Delta e_3/\Delta e_1)^2$ ratio becomes close to the experimental J_3/J_1 ratio when $x = 0.125$, for which $\Delta e_1 = 58$ meV, $\Delta e_2 = 25$ meV, and $\Delta e_3 = 17$ meV. From the equation $J_1 = -(\Delta e_1)^2/U_{eff}$ with $\Delta e_1 = 58$ meV and $J_1 = -22.5$ K, we obtain $U_{eff} = 1.74$ eV. Then, the J_2 and J_3 values are calculated to be −4.2 and −1.9 K, respectively, from the expression $J_i = -(\Delta e_i)^2/U_{eff}$ ($i = 2, 3$) with $\Delta e_2 = 25$ meV and $\Delta e_3 = 17$ meV.

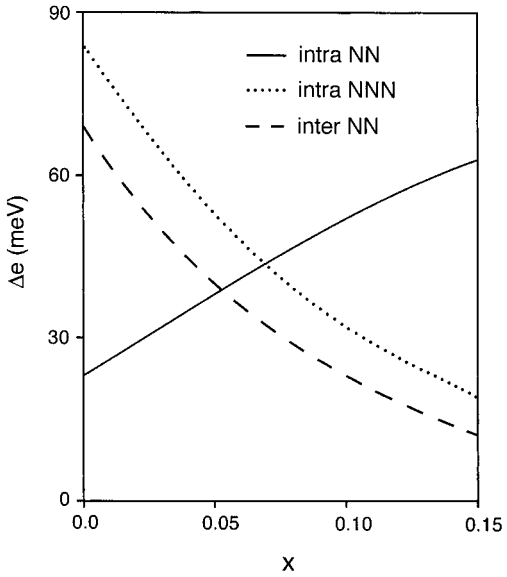

Figure 6. Δe values calculated for the intrachain NN, interchain NN, and intrachain NNN interactions in $LiCuVO_4$ as a function of the exponent $\zeta'(x) = 1.659(1 + x)$ of the diffuse STO in the DZ STO representation for the O 2p orbital.

It is noted that the calculated J_2/J_1 ratio (i.e., 0.19) for $LiCuVO_4$ is smaller than the critical value α_c (i.e., 0.241) found for a spin-$^1/_2$ Heisenberg chain with both NN and NNN antiferromagnetic interactions.[30,31] The ground state of such a chain is the spin liquid state characterized by no energy gap between the ground and the first excited states (as in the case of a spin-$^1/_2$ Heisenberg chain with only NN antiferromagnetic interactions) when $J_2/J_1 < \alpha_c$, but it is the dimer state characterized by nonzero energy gap between the ground and the first excited states when $J_2/J_1 > \alpha_c$.[30,31] Thus, the fact that the calculated J_2/J_1 ratio is smaller than α_c is consistent with the experimental finding that the CuO_2 ribbon chains of $LiCuVO_4$ undergo an antiferromagnetic ordering.[28,29]

As described previously, the use of $\zeta'(x)$ provides a satisfactory and consistent description of the spin exchange interactions of $LiCuVO_4$ when $x = 0.125$. Thus, we employ the $\zeta'(x = 0.125)$ value for the estimation of the spin exchange parameters for the intrachain NN (J_a), the intrachain NNN (J_b), and the interchain NN (J_c) interactions of the Cu_2O_3 lattices in Cu_4O_3 and $Ag_2Cu_2O_3$. Our results are summarized in Table 3, where the J values were calculated using the expression $J = -(\Delta e)^2/U_{eff}$ with the value of $U_{eff} = 1.74$ eV deduced for the magnetic lattice of $LiCuVO_4$.

5. Spin Ordering in the Cu_2O_3 Lattice Leading to Magnetic Phase Transition

5.1. Cu_4O_3. Table 3 reveals that the interchain NN interaction is more strongly antiferromagnetic than the intrachain NN interaction (i.e., $|J_c| > |J_a|$). This finding is explained by the fact that the Cu−O−Cu superexchange path has a significantly larger ∠Cu−O−Cu angle in the interchain

(29) Vasil'ev, A. N.; Ponomarenko, L. A.; Manaka, H.; Yamada, I.; Isobe, M.; Ueda, Y. *Physica B* **2000**, *284−286*, 1619.

(30) Okamoto, K.; Nomura, K. *Phys. Lett. A* **1992**, *169*, 433.

(31) Tonegawa, T.; Harada, I. *J. Phys. Soc. Jpn.* **1987**, *56*, 2153.

Table 3. ΔE and J Values Calculated for the Intrachain NN, Interchain NN, and Intrachain NNN Interactions of the Cu_2O_3 Lattices in Cu_4O_3 and $Ag_2Cu_2O_3$[a]

	Cu_4O_3[b]		$Ag_2Cu_2O_3$[c]	
interaction	e (meV)	J (K)	Δe (meV)	J (K)
intrachain NN (J_a)	51	−17.4	42	−11.8
intrachain NNN (J_b)	24	−3.9	22	−3.2
interchain NN (J_c)	85	−48.3	91	−55.4

[a] The J values were calculated using the expression $J = -(\Delta e)^2/U_{eff}$ with $U_{eff} = 1.74$ eV. [b] Calculated using the crystal structure of ref 1. [c] Calculated using the crystal structure of ref 6.

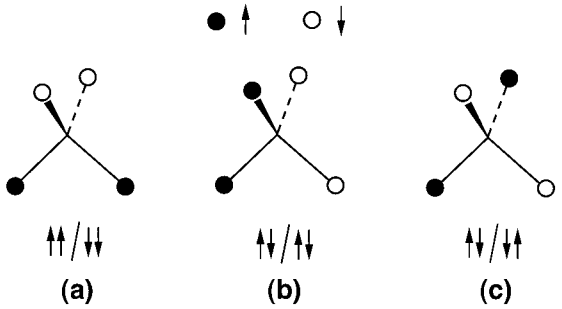

Figure 7. Three spin arrangements around a shared O(2) atom between adjacent CuO_2 ribbon chains: (a) ↑↑/↓↓, (b) ↑↓/↑↓, and (c) ↑↓/↓↑. Filled and empty circles represent the Cu^{2+} ions with up- and down-spins, respectively.

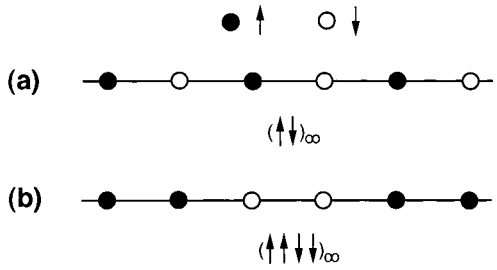

Figure 8. Two periodic spin arrangements in a CuO_2 ribbon chain: (a) $(\uparrow\downarrow)_\infty$ and (b) $(\uparrow\uparrow\downarrow\downarrow)_\infty$. Filled and empty circles represent the Cu^{2+} ions with up- and down-spins, respectively.

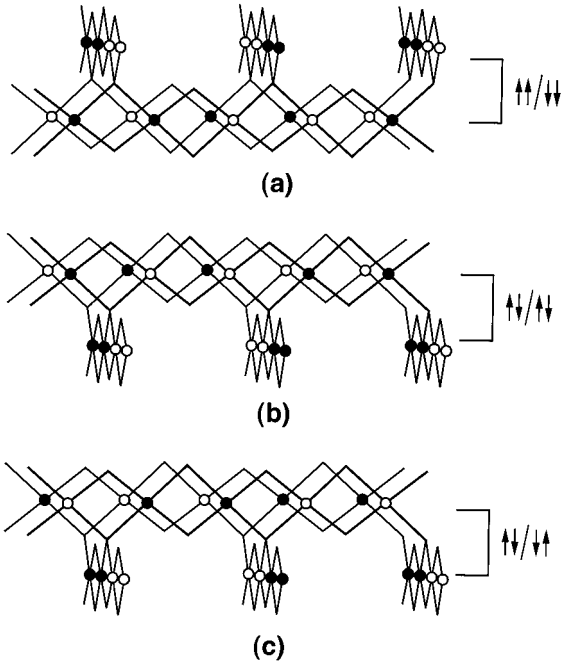

Figure 9. (a) Most favorable interchain spin arrangement between adjacent layers of CuO_2 ribbon chains, leading to a ↑↑/↓↓-double-layer. (b, c) Two equivalent interchain spin arrangements that can be used for the stacking between two ↑↑/↓↓-double-layers. Filled and empty circles represent the Cu^{2+} ions with up- and down-spins, respectively.

than in the intrachain NN interaction (Table 1). Table 3 also shows that the intrachain NN interaction is more strongly antiferromagnetic than the intrachain NNN interaction (i.e., $|J_a| > |J_b|$). Thus, the ordering of the spins in the Cu_2O_3 lattice of Cu_4O_3 should be determined primarily by the interchain NN interactions and then by the intrachain NN interactions. Each O(2) atom is the common bridging point of four interchain Cu−O−Cu superexchange paths (Figure 1b). Figure 7 depicts three arrangements of the four Cu^{2+} spins surrounding a single O(2) atom, that is, ↑↑/↓↓, ↑↓/↑↓ and ↑↓/↓↑. Because $|J_c|$ is larger than $|J_a|$, the ↑↑/↓↓ arrangement is more stable than the ↑↓/↑↓ and ↑↓/↓↑ arrangements. The latter two arrangements are equal in stability. Other possible interchain spin arrangements around O(2) (e.g., ↑↑/↑↓ and ↑↑/↑↑) are less stable than those shown in Figure 7. Two periodic spin arrangements of a CuO_2 ribbon chain, that is, $(\uparrow\downarrow)_\infty$ and $(\uparrow\uparrow\downarrow\downarrow)_\infty$, are shown in Figure 8. For a spin-$^1/_2$ Heisenberg chain with both NN and NNN antiferromagnetic interactions,[30,31] the spin arrangement $(\uparrow\uparrow\downarrow\downarrow)_\infty$ does not represent the ground state of the chain, regardless of whether the J_b/J_a ratio is smaller or larger than the critical value α_c. When J_a and J_b are both antiferromagnetic and $J_b/J_a < 1$, the $(\uparrow\downarrow)_\infty$ arrangement is more stable than the $(\uparrow\uparrow\downarrow\downarrow)_\infty$ arrangement. The most energetically favorable arrangement between two adjacent layers of CuO_2 ribbon chains is shown in Figure 9a, where every shared O(2) atom between the two layers has the interchain spin arrangement ↑↑/↓↓. This forces each CuO_2 ribbon chain to adopt the $(\uparrow\uparrow\downarrow\downarrow)_\infty$ spin arrangement and hence doubles the unit cell along the two chain directions, that is, the a- and b-directions.

To consider the spin ordering along the c-direction, we recall that the O(1) and O(2) atom alternations on the two edges of a CuO_2 ribbon chain have opposite senses (Figure 1b). Suppose that we add a layer of CuO_2 ribbon chains to a "↑↑/↓↓-double-layer" in which each shared O(2) atom has the interchain ↑↑/↓↓ arrangement (e.g., that shown in Figure 9a). Then, the new set of shared O(2) atoms generated by the additional layer can adopt either the spin arrangement in Figure 9b or that in Figure 9c, because the two interchain spin arrangements ↑↓/↑↓ and ↑↓/↓↑ available for the O(2) atoms are the same in energy. It is convenient to describe the spin ordering of the Cu_2O_3 lattice along the c-direction in terms of stacking ↑↑/↓↓-double-layers. Because the stacking between two ↑↑/↓↓-double-layers can achieved by adopting the ↑↓/↑↓ or ↑↓/↓↑ spin arrangement between them, the stacking of two ↑↑/↓↓-double-layers can lead to the "αα" arrangement shown in Figure 10a or the "$\alpha\beta$" arrangement shown in Figure 10b. The stacking of ↑↑/↓↓-double-layers can give rise to a large number of repeat patterns. The patterns such as $(\alpha\alpha)_\infty$ and $(\alpha\beta)_\infty$ do not double the unit cell along the c-direction, while the patterns such as $(\alpha\beta\alpha\alpha)_\infty$, $(\alpha\alpha\beta\alpha)_\infty$, $(\alpha\alpha\alpha\beta)_\infty$, $(\alpha\beta\beta\alpha)_\infty$, and $(\alpha\alpha\beta\beta)_\infty$ do. As an example, Figure 11 depicts the repeat pattern $(\alpha\beta\beta\alpha)_\infty$. In principle, the unit cell along the c-direction can be increased by a factor of any integer $n \geq$

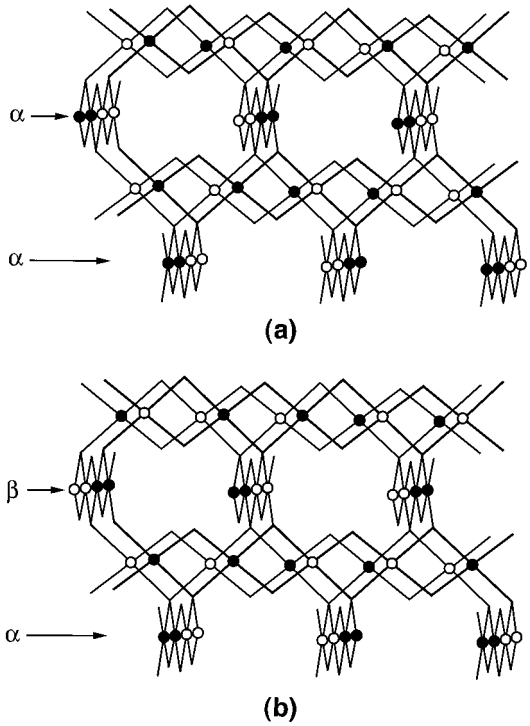

Figure 10. Two possible stacking arrangements between two ↑↑/↓↓-double-layers: (a) αα and (b) αβ. Filled and empty circles represent the Cu^{2+} ions with up- and down-spins, respectively.

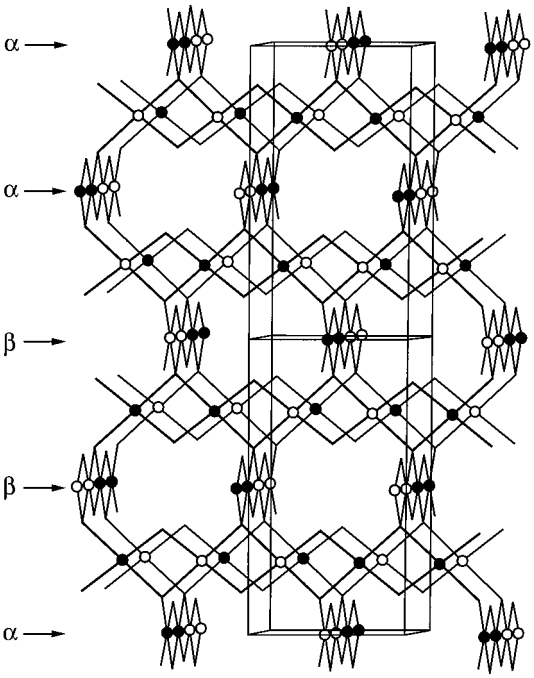

Figure 11. Stacking arrangement $(\alpha\beta\beta\alpha)_\infty$ in the Cu_2O_3 lattice that doubles the unit cell along the *a*-, *b*-, and *c*-directions. Filled and empty circles represent the Cu^{2+} ions with up- and down-spins, respectively. Each rectangular box represents a unit cell in the absence of the magnetic phase transition.

2. The experimental observation of the *c*-axis doubling is explained by noting that the spin orderings such as $(\alpha\beta\beta\alpha)_\infty$, $(\alpha\alpha\beta\beta)_\infty$, $(\beta\alpha\alpha\beta)_\infty$, and $(\beta\beta\alpha\alpha)_\infty$ are statistically the most probable arrangements, given the fact that the spin arrangements ↑↓/↑↓ and ↑↓/↓↑ are equally valid for the stacking between ↑↑/↓↓-double-layers.

This discussion of spin ordering along the *c*-direction leads to two important implications. First, the freedom of choice between the ↑↓/↑↓ and ↑↓/↓↑ arrangements for the stacking between ↑↑/↓↓-double-layers should give rise to spin fluctuation in the Cu_2O_3 spin lattice, and the extent of this spin fluctuation should depend on temperature. Second, the ordered spin arrangements of the Cu_2O_3 lattice that explain the observed superlattice formation differ from conventional antiferromagnetic ordering.

As already pointed out, the $(\uparrow\uparrow\downarrow\downarrow)_\infty$ spin ordering is not the most stable arrangement of an isolated CuO_2 ribbon chain. Thus, the interlayer ↑↑/↓↓ spin ordering around each O(2) atom, which induces the $(\uparrow\uparrow\downarrow\downarrow)_\infty$ spin ordering in the associated ribbon chains, would prevent the chains from adopting their most stable spin states. Namely, the interchain spin ordering frustrates the intrachain spin ordering, and vice versa. The extent of this magnetic frustration would be strongly enhanced if the J_a/J_c value were increased toward 1. If the J_a/J_c value were reduced toward 0, the magnetic structure of the Cu_2O_3 lattice would be dominated by the interchain spin ordering along the *c*-direction, thereby inducing a one-dimensional magnetic character. The calculated J_a/J_c value (i.e., 0.36) is closer to the limit of one-dimensional magnetism than to that of magnetic frustration, so that low-dimensional magnetic character would be more important than magnetic frustration in Cu_4O_3.

5.2. $Ag_2Cu_2O_3$. Table 3 reveals that the spin exchange parameters *J* calculated for $Ag_2Cu_2O_3$ are very similar to those calculated for Cu_4O_3, that is, $|J_c| > |J_a| > |J_b|$. Thus, it is expected that the magnetic phase transition of $Ag_2Cu_2O_3$ at 60 K should double the unit cell along each crystallographic direction, the Cu_2O_3 lattice of $Ag_2Cu_2O_3$ should exhibit spin fluctuation, and low-dimensional magnetic character would be more important than magnetic frustration for $Ag_2Cu_2O_3$.

Nevertheless, $Ag_2Cu_2O_3$ and Cu_4O_3 should show subtle differences because their J_a/J_c and J_b/J_a values are different. The $|J_c|$ value is slightly larger for $Ag_2Cu_2O_3$ than for Cu_4O_3, because the interchain Cu−O−Cu superexchange path has a slightly larger ∠Cu−O−Cu angle in $Ag_2Cu_2O_3$. The $|J_a|$ value is smaller for $Ag_2Cu_2O_3$ than for Cu_4O_3, because the two Cu−O−Cu intrachain superexchange paths are considerably more asymmetric in $Ag_2Cu_2O_3$. Consequently, $Ag_2Cu_2O_3$ has a smaller J_a/J_c value than does Cu_4O_3 (0.21 vs 0.36) so that $Ag_2Cu_2O_3$ should be more strongly affected by low-dimensional magnetic character than is Cu_4O_3. Another small difference between $Ag_2Cu_2O_3$ and Cu_4O_3 is that $J_b/J_a > \alpha_c$ for $Ag_2Cu_2O_3$ while $J_b/J_a < \alpha_c$ for Cu_4O_3 (i.e., 0.27 vs 0.22).

6. Concluding Remarks

In the Cu_2O_3 spin lattice of Cu_4O_3, the most favorable spin arrangement between adjacent layers of CuO_2 ribbon chains is ↑↑/↓↓, which forces the CuO_2 ribbon chains to adopt the $(\uparrow\uparrow\downarrow\downarrow)_\infty$ spin arrangement, hence doubling the unit cell along the *a*- and *b*-directions. The spin ordering along the *c*-direction is determined by the stacking of such ↑↑/↓↓-double-layers. The ordered spin arrangements in the Cu_2O_3 lattice

consistent with the observed superlattice formation are statistically the most probable arrangements, and they differ from conventional antiferromagnetic ordering. Because the spin arrangements ↑↓/↑↓ and ↑↓/↓↑ are equally valid for the stacking between ↑↑/↓↓-double-layers, there should occur spin fluctuation in the Cu_2O_3 lattice, the extent of which should depend on temperature. The calculated spin exchange parameters suggest that low-dimensional magnetic character is more important than magnetic frustration in determining the magnetic properties of Cu_4O_3. It would be interesting to examine spin fluctuation as a possible cause for the observed temperature dependence of a magnetic reflection intensity.[2] The spin exchange interactions of the Cu_2O_3 spin lattice in $Ag_2Cu_2O_3$ are very similar to those in Cu_4O_3. Thus, $Ag_2Cu_2O_3$ and Cu_4O_3 should be similar in their structural and magnetic properties.

Acknowledgment. The work at North Carolina State University was supported by the Office of Basic Energy Sciences, Division of Materials Sciences, U.S. Department of Energy, under Grant DE-FG02-86ER45259.

IC020141X